JACS
JOURNAL OF THE AMERICAN CHEMICAL SOCIETY
Article
pubs.acs.org/JACS

# Halide-Dependent Mechanisms of Reductive Elimination from Gold(III)

Matthew S. Winston, William J. Wolf, and F. Dean Toste*

Department of Chemistry, University of California, Berkeley, California 94720, United States

Supporting Information

**ABSTRACT:** Two unique organometallic halide series $(Ph_3P)Au(4\text{-}Me\text{-}C_6H_4)(CF_3)(X)$ and $(Cy_3P)Au(4\text{-}F\text{-}C_6H_4)(CF_3)(X)$ (X = I, Br, Cl, F) have been synthesized. The $PPh_3$-supported complexes can undergo both $C_{aryl}-X$ and $C_{aryl}-CF_3$ reductive elimination. Mechanistic studies of thermolysis at 122 °C reveal a dramatic reactivity and kinetic selectivity dependence on halide ligand. For X = I or F, zero-order kinetic behavior is observed, while for X = Cl or Br, kinetic studies implicate product catalysis. The selectivity for $C_{aryl}-CF_3$ bond formation increases in the order X = I < Br < Cl < F, with exclusively $C_{aryl}-I$ bond formation when X = I, and exclusively $C_{aryl}-CF_3$ bond formation when X = F. Thermodynamic measurements show that Au(III)−X bond dissociation energies increase in the order X = I < Br < Cl, and that ground state Au(III)−X bond strength ultimately dictates selectivities for $C_{aryl}-X$ and $C_{aryl}-CF_3$ reductive elimination.

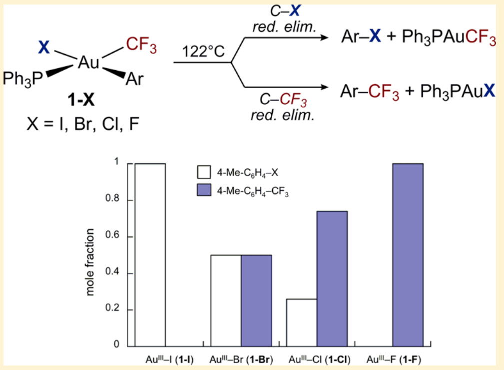


## INTRODUCTION

Transition metal-catalyzed transformations proceed through a series of fundamental steps, i.e., oxidative addition, migratory insertion, and reductive elimination. To minimize deleterious side reactions and maximize overall catalyst efficiency, the metal must undergo the proper series of reactions with excellent selectivity. A fundamental understanding of the factors that affect the selectivity of these elementary steps is critical in designing and improving new metal-catalyzed transformations.

We have recently shown[1] that complexes of the type $(Ph_3P)Au(aryl)$ (aryl = $4\text{-}F\text{-}C_6H_4$, $4\text{-}Me\text{-}C_6H_4$) undergo a photochemical oxidative addition to $CF_3I$ to give the air- and moisture-stable Au(III) complexes $(Ph_3P)Au(CF_3)(aryl)(I)$. These complexes undergo rapid $C_{aryl}-CF_3$ reductive elimination when treated with $AgSbF_6$ (Scheme 1). This transformation presumably proceeds via the cation $[(Ph_3P)Au(aryl)(CF_3)]^+$. Although this step demonstrates the oxidizing ability of Au(III) cations, a reliance on stoichiometric Ag(I) salts to generate the reactive cation is ultimately impractical if a catalytic process involving such Au(III) intermediates is to be realized. Due to our failed efforts to induce iodide dissociation either photochemically or with Lewis acids, we also investigated thermolytic routes,[1] and found that *neutral* $(Ph_3P)Au(aryl)(CF_3)(I)$ underwent solely $C_{aryl}-I$ reductive elimination at high temperatures (122 °C) (Scheme 1). Although $C_{aryl}-I$ reductive elimination from these complexes is facile, the factors controlling selectivity of C−X versus C−C bond formation are unclear due to a lack of other members of the halide family that could allow a comparative study.

**Scheme 1. Divergent Reductive Elimination Behavior of Au(III) Complexes**

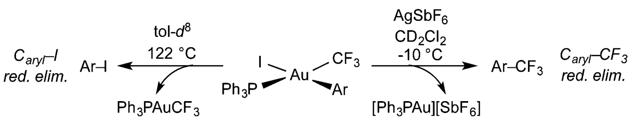


In a seminal study, Hartwig has shown that the rates of reversible $C_{aryl}-X$ reductive elimination from three-coordinate Pd(II) increase with halide polarizability (X = Cl < Br < I), while the thermodynamic driving force increases in the order X = I < Br < Cl.[2] However, because C−X (X = halide) reductive elimination is often endothermic, studies typically rely on using high-valent late metals such as Cu(III), Pd(IV) and Pt(IV) to establish a thermodynamic driving force.[3,4] In this vein, Au-catalyzed halogenations likely involve $C(sp^2)-X$ reductive elimination from Au(III),[5] and $C(sp^3)-F$[6] and $C(sp^3)-F$[7] eliminations from Au(III) have also been demonstrated.

$C_{aryl}-X$ reductive elimination is not necessarily productive, and may be a decomposition pathway for high-valent organometallic species with halide ligands. Importantly, Au(III) catalysts, which are often generated using dihalogen (or formal dihalogen) oxidants and stabilized by halide ligands,[8] could undergo deleterious, irreversible $C_{aryl}-X$ bond formation to deplete active catalyst concentrations. With access to a full family of Au(III) halides, trends in the rates of $C_{aryl}-X$ reductive elimination from Au(III) could be established. Perhaps slower $C_{aryl}-X$ bond formation could also be exploited to promote selectivity for otherwise challenging reductive eliminations, such as $C_{aryl}-CF_3$ bond formation in complexes of the type $(R_3P)Au(aryl)(CF_3)(X)$. Indeed, studies of *competitive*

**Received:** May 3, 2015
**Published:** June 11, 2015

  

DOI: 10.1021/jacs.5b04613
J. Am. Chem. Soc. 2015, 137, 7921−7928

reductive eliminations should inform factors dictating selectivity in catalytic cycles.[4c,k]

Herein, we report the synthesis and characterization of a series of well-defined complexes of the type $(R_3P)Au(aryl)(CF_3)(X)$ (X = I, Br, Cl, F) that undergo *both* $C_{aryl}$−X and $C_{aryl}$−$CF_3$ reductive elimination with different, halide-dependent kinetic ratios. These ratios vary systematically among the halide series, showing that halide ligands, often considered spectators, can dramatically influence reaction behavior.

## ■ RESULTS AND DISCUSSION

Sonicating **1-I** or **2-I** with excess AgX (X = Br, Cl, F) afforded metathesis products **1-X** and **2-X** (X = Br, Cl, F) in high yield (Scheme 2). Interestingly, **1-F** represents a rare example of an

**Scheme 2. Synthesis of Au(III) Halide Series**

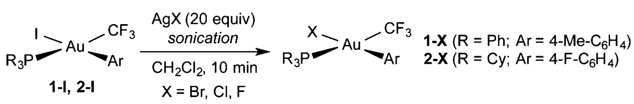


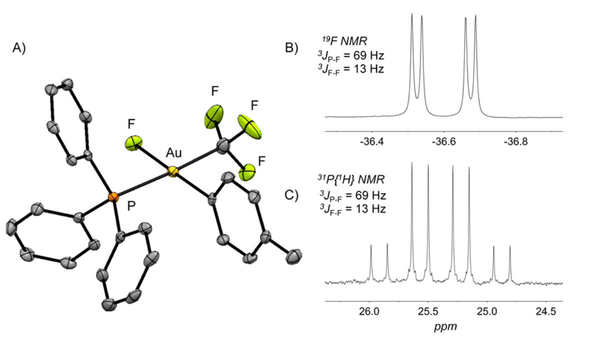


**Figure 1.** (A) Thermal ellipsoid representation of **1-F** at the 50% probability level. (B) $^{19}$F NMR signal corresponding to the Au−$CF_3$ functionality. (C) $^{31}P\{^1H\}$ NMR signal in $CD_2Cl_2$ corresponding to the Au-$PPh_3$ functionality.

isolable, terminal organometallic Au(III) fluoride (Figure 1). All complexes within the **1-X** halide series underwent thermolysis to products of $C_{aryl}$−X and $C_{aryl}$−$CF_3$ reductive elimination, and (when X = F) solvent activation. All reactions were followed by $^{19}$F NMR at 122 °C in toluene-$d^8$ ([**1-X**] = 14.0−16.0 mM). All values were quantified relative to 1-trifluoromethylnaphthalene ($^{19}$F δ: −59 ppm) as an internal standard. Due to irreversible formation of a new Au(III) species upon treatment with $[Bu_4N]X$ (presumably the aurates $[Bu_4N][Au(aryl)(CF_3)(X)_2]$ ($^{19}$F NMR singlet at δ −21 to −25 ppm), the kinetic order of halide anions could not be determined. Reactions run in the significantly more polar[9] $PhNO_2$ were only slightly affected (see Supporting Information), providing evidence against an ionic mechanism involving tight or dissociated ion pairs.

**Thermolysis of Au(III)−Iodide 1-I.** As previously reported, complex **1-I** underwent thermolysis at 122 °C to exclusively generate $Ph_3PAuCF_3$ and 4-Me-$C_6H_4$−I ($t_{1/2}$ = 2.5 min). Consumption of **1-I** followed unusual zero-order kinetics over a range of concentrations ($k_{obs} = 4.5 \times 10^{-5}$ M s$^{-1}$ from 6 to 35 mM [**1-I**], Figure 2 and Supporting Information Figure S1). When 0.005 equiv $PPh_3$ (70 μM) was added, the rate slowed substantially ($t_{1/2}$ = 28 min), and the reaction exhibited first-order behavior in **1-I** ($k_{obs} = 4.1 \times 10^{-5}$ s$^{-1}$). The observed rate constant ($k_{obs}$) is inverse first-order in $PPh_3$, implicating $PPh_3$ predissociation from **1-I** and reductive elimination from a short-lived three-coordinate Au(III) complex **3-I** under these conditions (Scheme 3). Consistent with this sequence, $PCy_3$-supported **2-I** did not react at 122 °C over 2 days, presumably due to the increased donor strength of the trialkylphosphine.

**Scheme 3. Proposed General Mechanism of $C_{aryl}$−X and $C_{aryl}$−$CF_3$ Reductive Eliminations from 1-X (X = I, Br, Cl, F)**

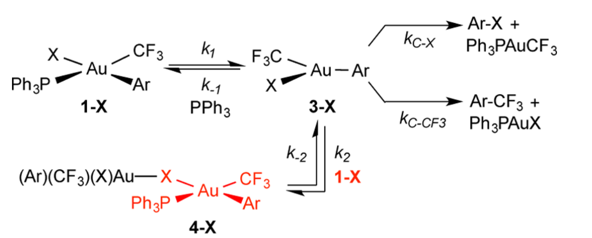


The zero-order kinetics in the absence of $PPh_3$ suggest reversible reaction inhibition by starting material. If reductive elimination proceeds through the coordinatively unsaturated **3-I**, a reasonable origin of this unusual behavior is trapping by **1-I** to μ-iodo bimetallic adduct **4-I** (Scheme 3). Indeed, μ-halide bridges between Au(III) atoms form readily to avoid coordinative unsaturation at the metal; in addition, bimetallic complexes such as $[AuCl_3]_2$, $[Me_2AuI]_2$, $[(F_3C)_2AuX]_2$ (X = I, Br), and $([SIPr)Au(Me)F]_2)^{2+}$ (SIPr = 1,3,-bis(2′,6′-

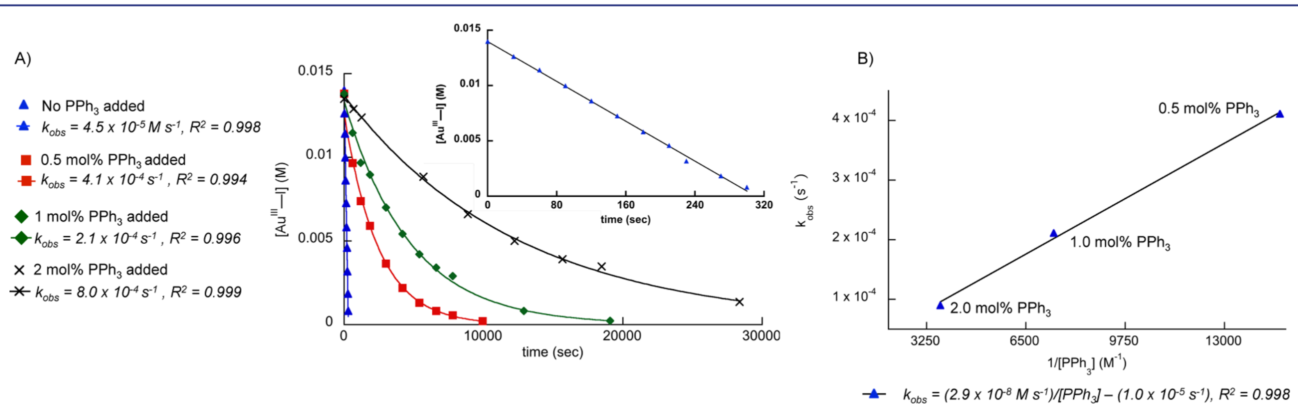


**Figure 2.** (A) Time courses for thermolysis of Au(III)−iodide **1-I** with 0, 0.5, 1.0, and 2.0 mol % $PPh_3$. Inset: Time course with 0 mol % added $PPh_3$. B) Inverse relationship between $k_{obs}$ and [$PPh_3$] indicating inverse first-order behavior of $PPh_3$ in the thermolysis of **1-I**.


DOI: 10.1021/jacs.5b04613
J. Am. Chem. Soc. 2015, 137, 7921−7928

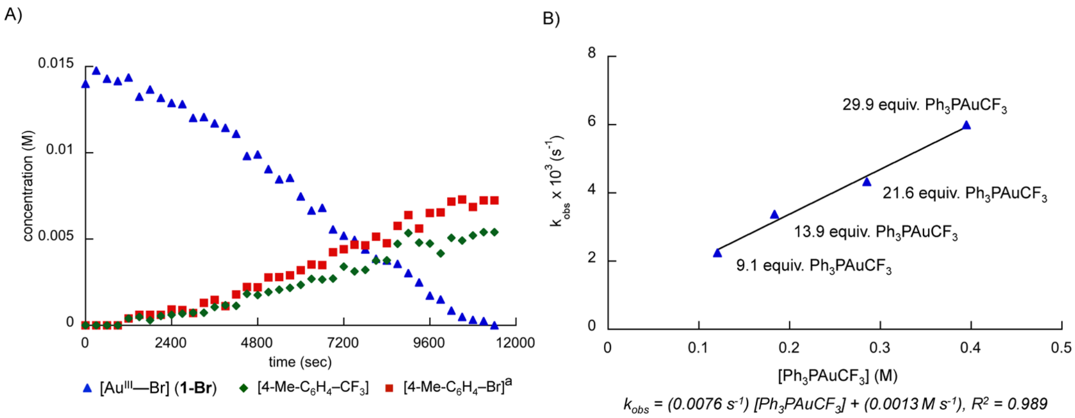


**Figure 3.** (A) Time course for thermolysis of Au(III)−bromide **1-Br** in the presence of 9.1−29.9 equiv of $Ph_3PAuCF_3$. (B) Direct relationship between $k_{obs}$ and $[Ph_3PAuCF_3]$ indicating first-order behavior of $Ph_3PAuCF_3$ in the thermolysis of **1-Br**.

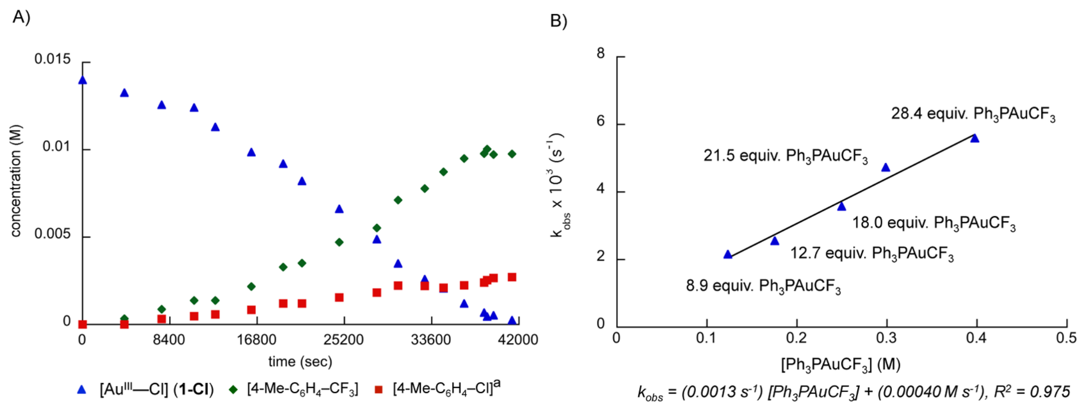


**Figure 4.** (A) Time course for thermolysis of Au(III)−chloride **1-Cl** in the presence of 8.9−28.4 equiv of $Ph_3PAuCF_3$. (B) Direct relationship between $k_{obs}$ and $[Ph_3PAuCF_3]$ indicating first-order behavior of $Ph_3PAuCF_3$ in the thermolysis of **1-Cl**.

diisopropylphenyl)imidazolin-2-ylidene) highlight the steric and electronic diversity that can complement $\mu$-halide interactions.[10]

Treating **3-I** as a steady-state intermediate, a complex rate law consistent with experimental observations can be derived (eq 1, see Supporting Information for derivation).

$$-\frac{d[\mathbf{1\text{-}I}]}{dt} = \frac{k_{C-I}(k_1[\mathbf{1\text{-}I}] + k_{-2}[\mathbf{4\text{-}I}])}{k_{-1}[PPh_3] + k_2[\mathbf{1\text{-}I}] + k_{C-I}} \qquad (1)$$

Since $[\mathbf{4\text{-}I}]$ must be less than $[\mathbf{3\text{-}I}]$, the assumption that $[\mathbf{4\text{-}I}] \approx 0$ is valid. If the formation of **4-I** is significantly faster than the recombination of $PPh_3$ and **3-I**, then $k_2[\mathbf{1\text{-}I}] \gg k_{-1}[PPh_3] + k_{C-I}$, and eq 1 simplifies to the zero-order rate law $-d[\mathbf{1\text{-}I}]/dt = k_{C-I}k_1/k_2$, which at 122 °C, is $4.5 \times 10^{-5}$ M s$^{-1}$.

In steady-state, $[PPh_3]$ must be very low. Since even small amounts of $PPh_3$ dramatically alter the reaction behavior, $k_{-1}$ must be substantially larger than $k_2$. Therefore, when $PPh_3$ is added, the rate law simplifies to

$$-\frac{d[\mathbf{1\text{-}I}]}{dt} = \frac{k_{C-I}k_1[\mathbf{1\text{-}I}]}{k_{-1}[PPh_3]} \qquad (2)$$

where $k_{C-I}k_1/k_{-1} = 2.9 \times 10^{-8}$ M s$^{-1}$. Thus, $k_{-1} = (1600)k_2$, in accordance with our previous conclusion that $k_{-1} \gg k_2$.

**Thermolyses of Au(III)−Bromide 1-Br and Au(III)−Chloride 1-Cl.** Qualitatively, the thermolyses of **1-Br** and **1-Cl** were notably slower ($t_{1/2} \sim 75$ and 400 min, respectively) than **1-I**, and products of *both* $C_{aryl}$−X and $C_{aryl}$−$CF_3$ reductive elimination were detected after full conversion ($[4\text{-Me-}C_6H_4\text{−}Br]/[4\text{-Me-}C_6H_4\text{−}CF_3]$ = 1.5:1 for **1-Br**, and $[4\text{-Me-}C_6H_4\text{−}Cl]/[4\text{-Me-}C_6H_4\text{−}CF_3]$ = 1:4.5 for **1-Cl**). To our surprise, reaction rates increased with time for both thermolyses (Figures 3A and 4A), suggestive of catalysis by products or nanoparticles.[11] Indeed, in the presence of excess $Ph_3PAuCF_3$, the rates of these thermolyses dramatically accelerated, behaving first-order in **1-Br** or **1-Cl** and $Ph_3PAuCF_3$ (Figures 3B and 4B, and see Supporting Information). The addition of 0.01 equiv (0.014 mM) $PPh_3$ dramatically slowed thermolysis of **1-Br** and **1-Cl** with and without excess $Ph_3PAuCF_3$, consistent with phosphine dissociation preceding reductive elimination in both the nonaccelerated and product-accelerated pathways.

Consistent with at least two processes with different product-determining steps, the ratios $[4\text{-Me-}C_6H_4\text{−}X]/[4\text{-Me-}C_6H_4\text{−}CF_3]$ vary over time during the thermolyses of **1-Br** and **1-Cl**. For instance, when $t < 20$ min, the accelerated pathway had not significantly contributed to consumption of **1-Br**, and there was almost no kinetic preference for $C_{aryl}$−Br or $C_{aryl}$−$CF_3$ bond formation ($[4\text{-Me-}C_6H_4\text{−}Br]/[4\text{-Me-}C_6H_4\text{−}CF_3]$ is roughly 1:1). However, in the presence of a large excess of $Ph_3PAuCF_3$ (140 mM), the accelerated pathway dominated even at early reaction times, and $C_{aryl}$−Br reductive elimination was slightly favored (2.3:1, presumably the intrinsic kinetic product distribution of the accelerated pathway.) For **1-Cl**, the product ratio $[4\text{-Me-}C_6H_4\text{−}Cl]/[4\text{-Me-}C_6H_4\text{−}CF_3]$ for the nonaccelerated pathway was roughly 1:2.8, while the accelerated


DOI: 10.1021/jacs.5b04613
J. Am. Chem. Soc. 2015, 137, 7921−7928

pathway heavily favored $C_{aryl}-CF_3$ reductive elimination (1:7.6).

We propose that the electron-withdrawing effect[12] of the $CF_3$ ligand renders $Ph_3PAuCF_3$ sufficiently Lewis acidic to coordinate the halide of **1-Br** or **1-Cl** in a $\mu$-bridging fashion,[13] effectively withdrawing electron density from the Au(III) center and perturbing the relative kinetic preferences for $C_{aryl}-X$ and $C_{aryl}-CF_3$ reductive elimination from **6-X**. Inhibition by $PPh_3$, the absence of saturation behavior at high $[Ph_3PAuCF_3]$, and unobservable intermediates suggest a process involving fast, reversible coordination of $Ph_3PAuCF_3$ to **1-Br** or **1-Cl**, followed by $PPh_3$ dissociation and slow $C_{aryl}-X$ and $C_{aryl}-CF_3$ reductive elimination (Scheme 4).

**Scheme 4. Proposed Mechanism for Accelerated Thermolysis of 1-X (X = Br, Cl)**

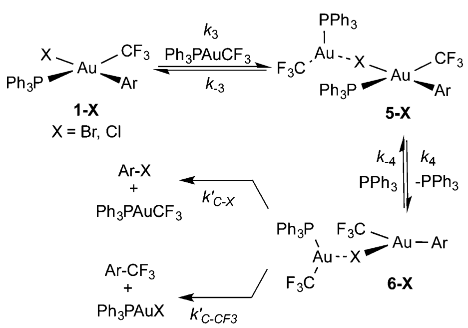

For both **1-Br** and **1-Cl**, kinetic details of the nonaccelerated pathway were masked by the accelerated reaction. However, the *slower* pathway is likely analogous to **1-I** thermolysis (Scheme 3), given the reaction's sensitivity to excess phosphine and the diversity of Au(III)-supported $\mu$-halide bridges.[11] The unambiguous first-order behavior in the presence of excess $Ph_3PAuCF_3$ clearly indicates that the accelerated reaction is substantially faster than the nonaccelerated process (see Supporting Information for rate laws.)

**Thermolysis of Au(III)–Fluoride 1-F.** The thermolysis of **1-F** was slower ($t_{1/2}$ = 33 min) than that of **1-I**, but significantly faster than that of **1-Br** and **1-Cl**. Consistent with the apparent trend of decreasing selectivity of $C_{aryl}-X$ reductive elimination in the order X = I > Br > Cl, we observed no 4-Me-$C_6H_4$–F upon heating **1-F**. Instead, 4-Me-$C_6H_4$–$CF_3$ was the major product. The formation of significant amounts of $d^7$ isotopologues of 2,4′-, 3,4′-, and 4,4′-dimethylbiphenyl (biaryl-$d^7$) and equimolar $Ph_3PAuCF_3$ suggest competitive activation of toluene-$d^8$ solvent and $C_{aryl}-C_{aryl}$ reductive elimination from a putative species Au(4-Me$C_6H_4$)(aryl-$d^7$)($CF_3$).[14,15] Since the ratio [4-Me-$C_6H_4$–$CF_3$]/[biaryl-$d^7$] remained constant (3.6:1) throughout the reaction, the rate laws for both $C_{aryl}-CF_3$ and $C_{aryl}-C_{aryl}$ reductive elimination must have the same molecularity to first approximation.

Although the selective $C_{aryl}-I$ reductive elimination from **1-I** stands in contrast to the selective $C_{aryl}-CF_3$ reductive elimination from **1-F**, the kinetic behavior for both thermolyses are notably similar. For instance, the thermolysis of **1-F** exhibited zero-order behavior (up to 80% conversion) (Figure 5) and was dramatically inhibited by $PPh_3$, consistent with slow $C_{aryl}-CF_3$ reductive elimination and slow solvent activation from three-coordinate intermediate **3-F**, which can be trapped by starting material (Scheme 3). Although solvent activation is in all likelihood a bimolecular process, [toluene-$d^8$] is essentially constant (~8.3 M at 122 °C in a sealed tube),[16] and the ratio of products expressed as rate terms $k_{C-CF3}/(k_{Ar}[\text{toluene-}d^8])$ is also constant (3.6) (Scheme 5). That **3-F** can activate solvent implicates an ionic Au(III)–F bond that imparts sufficient Lewis acidity for formal C–H activation by electrophilic aromatic substitution, fluoride-assisted deprotonation, or $\sigma$-bond metathesis.[17]

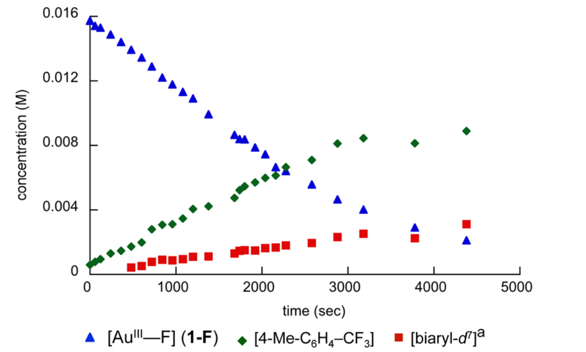


**Figure 5.** Time course for thermolysis of Au(III)–fluoride **1-F** exhibiting product catalysis. [a]Obtained by monitoring $[Ph_3PAuCF_3]$.

**Scheme 5. Proposed $C_{aryl}-CF_3$ and $C_{aryl}-C_{aryl}$ Coupling Reactions of Thermolysis Intermediate 3-F**

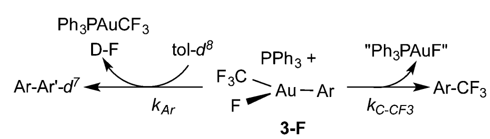

Like **1-I**, addition of 0.1 equiv $PPh_3$ (1.4 mM) slowed the reaction ($t_{1/2}$ = 300 min) and altered the order in **1-F** from zero to first (see Supporting Information ). However, only biaryl-$d^7$ was formed under these conditions, suggesting an alternative, *slower* solvent activation pathway that does not involve **3-F**. Although the Au(III) center in **1-F** is less electron-deficient and more sterically shielded than in **3-F** due to coordinative saturation, it may still be sufficiently Lewis acidic to activate solvent (Scheme 6). Consistent with this proposal, the reaction rate was independent of $[PPh_3]$ (from 1.4 to 14 mM), and the more electron-rich, sterically encumbered **2-F** did not react with toluene-$d^8$.

**Scheme 6. Proposed Mechanism of Solvent Activation and $C_{aryl}-C_{aryl}$ Coupling by 1-F**

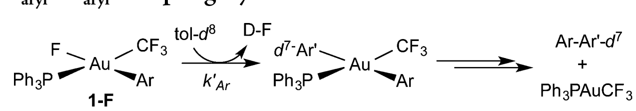

A rate law consistent with the mechanism of **1-F** thermolysis is shown in eq 3 where the zero-order term is significantly larger than the pseudo-first-order term in the absence of $PPh_3$, and $k_1(k_{C-CF3} + k_{Ar}[\text{tol-}d^8])/k_2$ = 3.9 × $10^{-6}$ M $s^{-1}$ (see Supporting Information for derivation).

$$-\frac{d[\mathbf{1\text{-}F}]}{dt} = \frac{k_1}{k_2}(k_{C-CF3} + k_{Ar}[\text{tol-}d^8]) + k'_{Ar}[\text{tol-}d^8][\mathbf{1\text{-}F}] \quad (3)$$

These kinetic investigations reveal that selectivity for $C_{aryl}-X$ versus $C_{aryl}-CF_3$ reductive elimination from Au(III) decreases in the order X = I > Br > Cl > F (Figure 6). While rate of $C_{aryl}-$



DOI: 10.1021/jacs.5b04613
J. Am. Chem. Soc. 2015, 137, 7921–7928

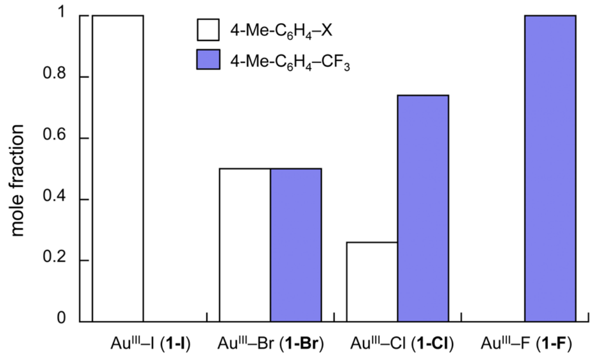


**Figure 6.** Distributions of products of reductive elimination from Au(III) halides **1-X**. For **1-Br** and **1-Cl**, these values represent the distributions of the *nonaccelerated* pathway.

X bond formation corresponds to halide polarizability,[7] thermodynamic studies were necessary to determine the role of ground state effects in the reaction selectivities.

**Relative Au(III)−X Bond Dissociation Enthalpies (X = I, Br, Cl).** To gain insight into what extent thermodynamics govern reductive elimination selectivity, van't Hoff analyses between **2-X** and trityl halides were carried out. The halide metathesis equilibria were monitored in toluene-$d^8$ by $^{19}F$ NMR at temperatures between 25 and 78 °C. Complexes **2-I** and **2-Br** were treated with an excess of $Ph_3C-Cl$ (30 equiv) to ensure fast approach to equilibrium, and to hold [$Ph_3C-Cl$] constant for determination of the equilibrium constant.[18] The equilibrium between **2-Cl** (+ $Ph_3C-I$) and **2-I** (+ $Ph_3C-Cl$) was moderately exothermic ($\Delta H^o$ = −4.8 kcal/mol) with a negligible loss of entropy ($\Delta S^o$ = −2.1 e.u.) (Figure 7).

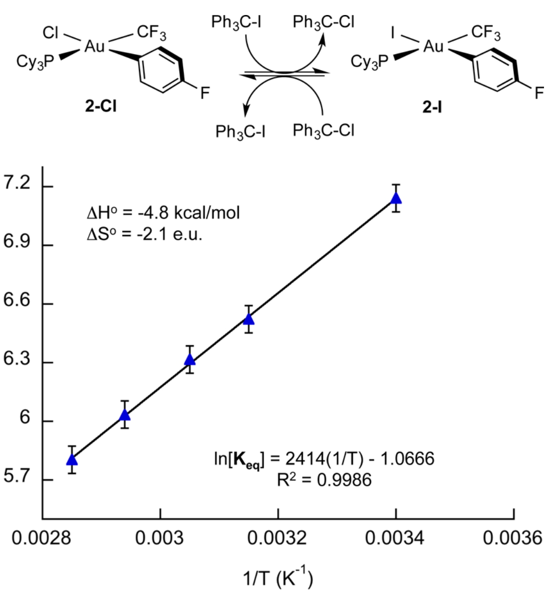


**Figure 7.** van't Hoff plot of the equilibrium of **2-Cl** (+ $Ph_3C-I$) and **2-I** (+ $Ph_3C-Cl$) (shown above) in toluene-$d^8$ between 25 and 78 °C. Initial conditions: **2-I** + $Ph_3C-Cl$ (30 equiv).

Similarly, the equilibrium between **2-Cl** (+ $Ph_3C-Br$) and **2-Br** (+ $Ph_3C-Cl$) also lies to the right ($\Delta H^o$ = −3.1 kcal/mol) with a negligible entropy loss ($\Delta S^o$ = −1.8 e.u.) (Figure 8).

Using the thermodynamic parameters above, and differences in Benson group increments for tertiary alkyl halide groups (see Supporting Information for derivation),[19] we obtain the

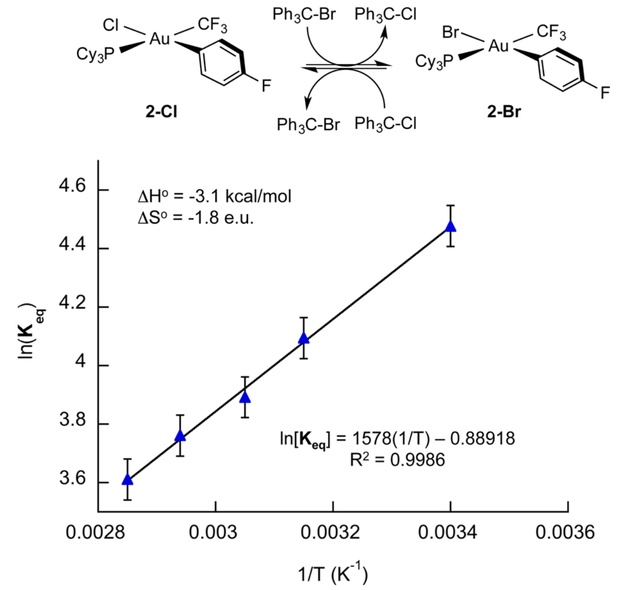


**Figure 8.** van't Hoff plot of the equilibrium of **2-Cl** (+ $Ph_3C-Br$) and **2-Br** (+ $Ph_3C-Cl$) (shown above) in toluene-$d^8$ between 25 and 78 °C. Initial conditions: **2-Br** + $Ph_3C-Cl$ (30 equiv).

differences in heats of formation ($\Delta\Delta H^o_f$) of **2-Cl**, **2-Br**, and **2-I**: $\Delta H^o_f$(**2-I**) is 13 kcal/mol greater than $\Delta H^o_f$(**2-Br**), and 21 kcal/mol greater than $\Delta H^o_f$(**2-Cl**).

The differences in bond dissociation energies (ΔBDE) of each Au(III)−X bond are functions of $\Delta\Delta H^o_f$ (**2-X**) and BDEs of the diatomic halogens (see Supporting Information for derivation).[20] Although rough approximations, these values suggest that the Au(III)−I bond in **2-I** is 18 kcal/mol weaker than the Au(III)−Br bond in **2-Br**, and 33 kcal/mol weaker than the Au(III)−Cl bond in **2-Cl**.[21] The trend in Au(III)−X bond strengths follows $C_{aryl}-X$ bond strengths, with the variation in Au(III)−X BDEs only slightly greater. That the bond dissociation energies decrease in the order Au(III)−Cl > Au(III)−Br > Au(III)−I suggests that selectivities for $C_{aryl}-X$ and $C_{aryl}-CF_3$ reductive elimination are strongly influenced by the strength of the Au(III)−X bond in the starting material (Figure 8), and that Au−X bonding must be substantially diminished in the transition state to $C_{aryl}-X$ reductive elimination. Halide polarizability, or softness, is correlated with nucleophilicity, and may also play a role in dictating relative rates of $C_{aryl}-X$ bond formation, as noted by Hartwig for Pd(II) systems.[2]

## ■ CONCLUSIONS

We have accessed full Au(III) halide families through formal oxidative addition of $CF_3I$ to Au(I) followed by halide metathesis, and have systematically studied the thermolysis of **1-X** (X = F, Cl, Br, I) and the competitive $C_{aryl}-X$ and $C_{aryl}-CF_3$ reductive eliminations from Au(III). The mechanisms and kinetic selectivities for these steps are highly dependent on the identity of the halide ligand. When X = I, thermolysis exclusively generates the products of $C_{aryl}-I$ bond formation. The selectivity for $C_{aryl}-CF_3$ reductive elimination increases in the order X = I < Br < Cl < F, and is completely selective for $C_{aryl}-CF_3$ bond formation when X = F (Figure 6). Thermodynamic studies reveal that the Au(III)−X bond strength increases in the order X = I < Br < Cl, a trend that mirrors selectivity for $C_{aryl}-CF_3$ reductive elimination. These


DOI: 10.1021/jacs.5b04613
J. Am. Chem. Soc. 2015, 137, 7921−7928

observations suggest that selectivity for reductive elimination is strongly dictated by the Au(III)−X bond strength in the reactant, and possibly halide polarizability. Highlighting stark reactivity differences between fluoride and higher halide ligands, we have also shown that the Au(III)−F bond is relatively ionic, and can activate C−H/D bonds in arene solvent at elevated temperatures. Surprisingly, the thermolyses of **1-Br** and **1-Cl** are accelerated by $Ph_3PAuCF_3$, presumably via coordination of $Ph_3PAuCF_3$ to the Au(III)−bound halide.

In conclusion, $C_{aryl}$−X reductive elimination can be facile from Au(III) at elevated temperatures, a process that is rarely observable and probed systematically at other $d^8$ metal centers.[2,3] Depending on the nature of the halide ligand, this process can outcompete $C_{aryl}$−$CF_3$ bond formation. Thus, irreversible $C_{aryl}$−X reductive elimination should not be discounted as a possible, deleterious thermodynamic sink in studies of organometallic Au(III) halides or Au(I) under oxidative conditions. These studies also suggest that challenging $C_{aryl}$−C reductive elimination from Au(III) halides is favored when X = Cl or F, due to relatively stronger Au(III)−X bonds compared to the higher halides. More broadly, reductive elimination is a fundamental step in many catalytic cycles, and judicious choice of halide, often considered a spectator ligand, may in fact be essential to achieving challenging C−C bond formation.

## ■ METHODS

**General Considerations.** Unless otherwise stated, all manipulations were carried out at ambient temperature (20 °C) under an atmosphere of purified nitrogen in a Vacuum Atmospheres Corp. glovebox or with a double manifold vacuum line using standard Schlenk techniques. All glassware was dried at 150 °C for 12 h prior to use. Solvents were dried by passage through a column of activated alumina under nitrogen pressure and degassed by sparging with dry nitrogen. Toluene-$d^8$ was distilled from sodium ketyl. $CF_3I$ was purchased from Oakwood and connected to a double-manifold vacuum line fitted with Hg manometers to regulate pressure. AgI, AgBr, and AgCl were prepared by treating $AgNO_3$ with the respective NaX (X = halide) salt in water at room temperature, then filtering and drying. AgF was purchased from Strem and used without further purification. $Ph_3C$−Cl and $Ph_3C$−Br were purchased from Sigma-Aldrich and used as received. $Ph_3C$−F was prepared according to literature procedure.[22] $(Ph_3P)Au(4\text{-Me-}C_6H_4)(CF_3)(I)$ (**1-I**), $(Cy_3P)Au(4\text{-F-}C_6H_4)(CF_3)(I)$ (**2-I**), and $Ph_3PAuCF_3$ were prepared according to a recent publication from our lab.[1]

NMR spectra were recorded using Bruker AVQ-400, DRX-500, AV-500 or AV-600 spectrometers, and chemical shifts are referenced to residual NMR solvent peaks ($^1$H and $^{13}$C), 1-$CF_3$-naphthalene ($^{19}$F), or $H_3PO_4$ ($^{31}$P). Elemental analyses were performed at the College of Chemistry Microanalytical Laboratory, University of California, Berkeley. X-ray structural determinations were performed at CheXray, University of California, Berkeley on Bruker SMART 1000 or SMART APEX diffractometers.

**Improved Procedure for the Synthesis of 1-I and 2-I.** A 25 mL Pyrex Schlenk tube was charged with $Ph_3PAu(4\text{-Me-}C_6H_4)$ or $Cy_3PAu(4\text{-F-}C_6H_4)$ (up to 3 mmol) and the solid was dissolved in $CH_2Cl_2$ to give a 0.2 M solution. The tube was sealed and degassed with three freeze−pump−thaw cycles. $CF_3I$ gas was introduced (1 atm) and the reaction vessel was sealed and placed in direct sunlight for 15 min. The reaction mixture turned yellow within seconds of irradiation. After irradiation, the excess $CF_3I$ was vented and the reaction mixture adsorbed to neutral alumina and concentrated to dryness. The alumina mixture was then loaded onto a silica column and the desired Au(III) compounds were eluted in benzene/hexanes (1:1 (v/v), $R_f$ = 0.2 for **1-I**; $R_f$ = 0.55 for **2-I**). Yields typically range between 60 and 90%. All spectroscopic data match those previously reported.[1]

**Halide Metathesis between 1-I or 2-I with AgX.** **1-I** (75 mg, 0.10 mmol) or **2-I** (77 mg, 0.10 mmol) was dissolved in $CH_2Cl_2$ (5 mL) in a vial. AgX (X = Br, Cl, F) (1.0 mmol) was added at once, and the reaction was capped and sonicated for 5 min in the dark, followed by a second addition of AgX (1.0 mmol) and further sonication for 5 min. When X = Br or Cl, the solid turned increasingly yellow with the formation of AgI. The suspension was filtered through a bed of Celite and concentrated *in vacuo* to a white powder that was recrystallized twice in 1:3 $CH_2Cl_2$/pentane to afford **1-Br** (52 mg, 0.074 mmol), **2-Br** (61 mg, 0.081 mmol), **1-Cl** (51 mg, 0.078 mmol), **2-Cl** (60 mg, 0.089 mmol), **1-F** (45 mg, 0.071 mmol), or **2-F** (55 mg, 0.083 mmol) in analytical purity as white solids.

*$(Ph_3P)Au(4\text{-Me-}C_6H_4)(CF_3)(Br)$* ***(1-Br)***. $^1$H NMR ($CD_2Cl_2$, 500 MHz, $\delta$): 7.54−7.49 (m, 3H), 7.46−7.35 (m, 12H), 6.77 (d, $J$ = 8.4 Hz, 2H), 6.64 (d, $J$ = 8.4 Hz, 2H), 2.15 (s, 3H). $^{13}$C{$^1$H} NMR ($CD_2Cl_2$, 125 MHz, $\delta$): 135.9, 134.9 (d, $J$ = 10 Hz), 132.2 (d, $J$ = 3 Hz), 130.7 (d, $J$ = 3 Hz), 130.6, 129.1 (d, $J$ = 11 Hz), 126.2, 125.7, 20.6. *ipso*-$^{13}$C signals not observed due to heteroatom coupling. $^{31}$P{$^1$H} NMR ($CD_2Cl_2$, 162 MHz, $\delta$): 24.2 (q, $^3J_{P-F}$ = 68 Hz). $^{19}$F NMR ($CD_2Cl_2$, 376 MHz, $\delta$): −27.6 (d, $^3J_{P-F}$ = 68 Hz). Anal. Calcd for $C_{26}H_{22}AuBrF_3P$: C, 44.66; H, 3.17. Found: C, 44.94; H, 3.33.

*$(Cy_3P)Au(4\text{-F-}C_6H_4)(CF_3)(Br)$* ***(2-Br)***. $^1$H NMR ($CD_2Cl_2$, 500 MHz, $\delta$): 7.31−7.26 (m, 2H), 7.01−6.96 (m, 2H), 2.38−2.26 (m, 3H), 1.91−1.76 (m, 12H), 1.73−1.55 (m, 9H), 1.32−1.20 (m, 3H), 1.14−1.00 (m, 6H). $^{13}$C{$^1$H} NMR ($CD_2Cl_2$, 125 MHz, $\delta$): 161.7 (d, $J$ = 246 Hz), 139.3−139.1 (m), 133.0 (dd, $J$ = 6 Hz, $J$ = 1 Hz), 116.3 (d, $J$ = 20 Hz), 34.1 (d, $J$ = 25 Hz), 29.8 (d, $J$ = 3 Hz), 27.6 (d, $J$ = 11 Hz), 26.3 (d, $J$ = 1 Hz). *ipso*-$^{13}$C signals not observed due to heteroatom coupling. $^{31}$P{$^1$H} NMR ($CD_2Cl_2$, 162 MHz, $\delta$): 28.0 (q, $^3J_{P-F}$ = 64 Hz). $^{19}$F NMR ($CD_2Cl_2$, 376 MHz, $\delta$): −29.5 (d, $^3J_{P-F}$ = 63 Hz, Au−$CF_3$), −117.3 − −117.4 (m, Ar-*F*). Anal. Calcd for $C_{25}H_{37}AuBrF_4P$: C, 41.62; H, 5.17. Found: C, 41.47; H, 5.33.

*$(Ph_3P)Au(4\text{-Me-}C_6H_4)(CF_3)(Cl)$* ***(1-Cl)***. $^1$H NMR ($CD_2Cl_2$, 500 MHz, $\delta$): 7.55−7.50 (m, 3H), 7.44−7.35 (m, 12H), 6.79 (d, $J$ = 8.1 Hz, 2H), 6.64 (d, $J$ = 8.1 Hz, 2H), 2.15 (s, 3H). $^{13}$C{$^1$H} NMR ($CD_2Cl_2$, 125 MHz, $\delta$): 140.0, 134.8 (d, $J$ = 11 Hz), 132.2 (d, $J$ = 3 Hz), 131.0 (d, $J$ = 3 Hz), 130.7, 129.2 (d, $J$ = 11 Hz), 125.8, 125.3, 20.6. *ipso*-$^{13}$C signals not observed due to heteroatom coupling. $^{31}$P{$^1$H} NMR ($CD_2Cl_2$, 162 MHz, $\delta$): 25.6 (q, $^3J_{P-F}$ = 69 Hz). $^{19}$F NMR ($CD_2Cl_2$, 376 MHz, $\delta$): −30.5 (d, $^3J_{P-F}$ = 69 Hz). Anal. Calcd for $C_{26}H_{22}AuClF_3P$: C, 47.69; H, 3.39. Found: C, 47.75; H, 3.51.

*$(Cy_3P)Au(4\text{-F-}C_6H_4)(CF_3)(Cl)$* ***(2-Cl)***. $^1$H NMR ($CD_2Cl_2$, 500 MHz, $\delta$): 7.34−7.30 (m, 2H), 7.00−6.96 (m, 2H), 2.33−2.22 (m, 3H), 1.90−1.76 (m, 12H), 1.73−1.58 (m, 9H), 1.32−1.21 (m, 3H), 1.14−1.02 (m, 6H). $^{13}$C{$^1$H} NMR ($CD_2Cl_2$, 125 MHz, $\delta$): 161.6 (d, $J$ = 243 Hz), 136.6−136.4 (m), 133.2 (dd, $J$ = 7 Hz, $J$ = 1 Hz), 116.4 (d, $J$ = 21 Hz), 33.5 (d, $J$ = 25 Hz), 29.6 (d, $J$ = 2 Hz), 27.7 (d, $J$ = 11 Hz), 26.3 (d, $J$ = 1 Hz). *ipso*-$^{13}$C signals not observed due to heteroatom coupling. $^{31}$P{$^1$H} NMR ($CD_2Cl_2$, 162 MHz, $\delta$): 28.7 (q, $^3J_{P-F}$ = 64 Hz). $^{19}$F NMR ($CD_2Cl_2$, 376 MHz, $\delta$): −32.8 (d, $^3J_{P-F}$ = 64 Hz, Au−$CF_3$), −117.4 − −117.5 (m, Ar-*F*). Anal. Calcd for $C_{25}H_{37}AuClF_4P$: C, 44.36; H, 5.51. Found: C, 44.29; H, 5.40.

*$(Ph_3P)Au(4\text{-Me-}C_6H_4)(CF_3)(F)$* ***(1-F)***. $^1$H NMR ($CD_2Cl_2$, 500 MHz, $\delta$): 7.56−7.51 (m, 3H), 7.49−7.43 (m, 6H), 7.43−7.37 (m, 6H), 6.77 (dd, $J$ = 8.2 Hz, $J$ = 3.3 Hz, 2H), 6.60 (d, $J$ = 8.0 Hz, 2H), 2.15 (s, 3H). $^{13}$C{$^1$H} NMR ($CD_2Cl_2$, 125 MHz, $\delta$): 135.9, 134.6 (dd, $J$ = 11 Hz, $J$ = 2 Hz), 132.4 (d, $J$ = 3 Hz), 131.3 (dd, $J$ = 5 Hz, $J$ = 2 Hz), 130.2 (d, $J$ = 5 Hz), 129.4 (d, $J$ = 11 Hz), 125.5, 125.0, 20.6. *ipso*-$^{13}$C signals not observed due to heteroatom coupling. $^{31}$P{$^1$H} NMR ($CD_2Cl_2$, 162 MHz, $\delta$): 25.4 (qd, $^3J_{P-F}$ = 69 Hz, $^2J_{P-F}$ = 28 Hz). $^{19}$F NMR ($CD_2Cl_2$, 376 MHz, $\delta$): −36.6 (dd, $^3J_{P-F}$ = 70 Hz, $^3J_{F-F}$ = 13 Hz), −236.4 − −236.6 (m). Anal. Calcd for $C_{26}H_{22}AuF_4P$: C, 48.92; H, 3.47. Found: C, 48.64; H, 3.68.

*$(Cy_3P)Au(4\text{-F-}C_6H_4)(CF_3)(F)$* ***(2-F)***. $^1$H NMR ($CD_2Cl_2$, 500 MHz, $\delta$): 7.30−7.24 (m, 2H), 6.96−6.90 (m, 2H), 2.24−2.12 (m, 3H), 1.92−1.76 (m, 12H), 1.75−1.53 (m, 9H), 1.34−1.21 (m, 3H), 1.17−1.05 (m, 6H). $^{13}$C{$^1$H} NMR ($CD_2Cl_2$, 125 MHz, $\delta$): 161.7 (d, $J$ = 244 Hz), 133.4−133.2 (m), 116.1 (dd, $J$ = 21 Hz, $J$ = 5 Hz), 32.6 (d, $J$ = 24 Hz), 29.4 (d, $J$ = 2 Hz), 27.6 (d, $J$ = 11 Hz), 26.2 (d, $J$ = 1 Hz) *ispo*-$^{13}$C signals not observed due to heteroatom coupling. $^{31}$P{$^1$H} NMR



DOI: 10.1021/jacs.5b04613
J. Am. Chem. Soc. 2015, 137, 7921−7928

($CD_2Cl_2$, 162 MHz, $\delta$): 33.2 (qd, $^3J_{P-F}$ = 65 Hz, $^2J_{P-F}$ = 23 Hz). $^{19}$F NMR ($CD_2Cl_2$, 376 MHz, $\delta$): −39.3 (dd, $^3J_{P-F}$ = 64 Hz, $^3J_{F-F}$ = 13 Hz, Au−$CF_3$), −117.8 − −117.9 (m, Ar-*F*), −249.0 − −249.2 (m). Anal. Calcd for $C_{25}H_{37}AuF_5P$: C, 45.46; H, 5.65. Found: C, 45.21; H, 5.36.

**Kinetic Experiments.** A 14−16 mM solution of **1-X** in tol-$d^8$ was prepared in an inert atmosphere glovebox. Standard (1-trifluoromethylnaphthalene) was added by microsyringe, and 500 $\mu$L aliquots of the solution were transferred to oven-dried NMR tubes. The tubes were capped with greased rubber septa and sealed with Teflon tape. When appropriate, $PPh_3$ or $Ph_3PAuCF_3$ were added directly to the NMR tube as a solid prior to injection of the tol-$d^8$ solution of **1-X** and standard.

The thermolyses of **1-I** and **1-F** were carried out in a Bruker DRX-500 NMR probe that was temperature calibrated using ethylene glycol and preheated to 122 °C for 30 min. The spectrometer was shimmed and tuned with a solution of standard, then the NMR tube containing the solution of interest was lowered into the probe. All other reactions were carried out at 122 °C in an oil bath shielded from light and the samples were periodically removed from the bath, cooled to room temperature, and monitored by $^{19}$F NMR.

**Thermodynamic Experiments.** A 14−16 mM solution **2-X** in tol-$d^8$ was prepared in an inert atmosphere glovebox. Standard (3,5-ditrifluoromethyl-1-bromobenzene) was added by microsyringe, and 500 $\mu$L aliquots of the solution were transferred to oven-dried NMR tubes charged with $Ph_3C$−Cl (63 mg, 0.23 mmol). The tubes were capped with greased rubber septa and sealed with Teflon tape. All experiments were heated in an NMR probe that was calibrated as described above. The equilibria were first monitored at 25 °C after 10 min at room temperature. After each increase in temperature, the probe was recalibrated, and the solution of interest was heated in the probe for 10 min. After equilibrium at maximum temperature (78 °C) was reached, the reaction was cooled to 25 °C and the equilibrium was measured.

## ■ ASSOCIATED CONTENT

### Supporting Information

Experimental details, characterization data, and crystallographic information (cif). The Supporting Information is available free of charge on the ACS Publications website at DOI: 10.1021/jacs.5b04613.

## ■ AUTHOR INFORMATION


### Corresponding Author

*fdtoste@berkeley.edu


### Notes

The authors declare no competing financial interest.

## ■ ACKNOWLEDGMENTS

We gratefully acknowledge Professor Robert G. Bergman, Andrew Samant, and David Kaphan for helpful discussions. This work was generously funded by the NIHGMS (RO1 GM073932), a NIH fellowship to M.S.W. (F32 GM103238-02) and an NSF fellowship to W.J.W. (DGE 1106400). X-ray crystallography was performed using the UC Berkeley College of Chemistry CheXray facility supported by the NIH Shared Instrumentation Grant S10- RR027172; we thank Guoqing Geng and the Chemistry 208 class at UC Berkeley for assistance with the X-ray structure of **1-Cl**.

## ■ REFERENCES


(1) Winston, M. S.; Wolf, W. J.; Toste, F. D. *J. Am. Chem. Soc.* **2014**, *136*, 7777.

(2) Roy, A. H.; Hartwig, J. F. *J. Am. Chem. Soc.* **2003**, *125*, 13944.

(3) (a) Klapars, A.; Buchwald, S. L. *J. Am. Chem. Soc.* **2002**, *124*, 14844. (b) Zanon, J.; Klapars, A.; Buchwald, S. L. *J. Am. Chem. Soc.* **2003**, *125*, 2890. (c) Casitas, A.; Poater, A.; Solà, M.; Stahl, S. S.; Costas, M.; Ribas, X. *Dalton Trans.* **2010**, *39*, 10458. (d) Lin, B.-L.; Kang, P.; Stack, T. D. P. *Organometallics* **2010**, *29*, 3683. (e) For a review see: Sheppard, T. D. *Org. Biomol. Chem.* **2009**, *7*, 1043.

(4) (a) Dekleva, T. W.; Forster, D. *Adv. Catal.* **1986**, *34*, 81. (b) Goldberg, K. I.; Yan, J.; Winter, E. L. *J. Am. Chem. Soc.* **1994**, *116*, 1573. (c) Goldberg, K. I.; Yan, J.; Breitung, E. M. *J. Am. Chem. Soc.* **1995**, *117*, 6889. (d) Maitlis, P. M.; Haynes, A.; Sunley, G. J.; Howard, M. J. *J. Chem. Soc., Dalton Trans.* **1996**, 2187. (e) Frech, C. M.; Milstein, D. *J. Am. Chem. Soc.* **2006**, *128*, 12434. (f) Whitfield, S. R.; Sanford, M. S. *J. Am. Chem. Soc.* **2007**, *129*, 15142. (g) Furuya, T.; Ritter, T. *J. Am. Chem. Soc.* **2008**, *130*, 10060. (h) Racowski, J. M.; Gary, B. G.; Sanford, M. S. *Angew. Chem., Int. Ed.* **2012**, *51*, 3414. (i) O'Reilly, M. E.; Pahls, D. R.; Cundari, T. R.; Gunnoe, T. B. *Organometallics* **2014**, *33*, 6504. (j) Rivada-Wheelaghan, O.; Roselló-Merino, M.; Díez, J.; Maya, C.; López-Serrano, J.; Conejero, S. *Organometallics* **2014**, *33*, 5944. (k) Pérez-Temprano, M. H.; Racowski, J. M.; Kampf, J. W.; Sanford, M. S. *J. Am. Chem. Soc.* **2014**, *136*, 4097. (l) Camasso, N. M.; Sanford, M. S. *Science* **2015**, *347*, 1218.

(5) For examples, see: (a) Qiu, D.; Mo, F.; Zheng, Z.; Zhang, Y.; Wang, J. *Org. Lett.* **2010**, *12*, 5475. (b) Nguyen, K. H.; Tomasi, S.; Le Roch, M.; Toupet, L.; Renault, J.; Uriac, P.; Gouault, N. *J. Org. Chem.* **2013**, *78*, 7809.

(6) Mankad, N. P.; Toste, F. D. *Chem. Sci.* **2012**, *3*, 72.

(7) Scott, V. J.; Labinger, J. A.; Bercaw, J. E. *Organometallics* **2010**, *29*, 4090.

(8) See references contained in: Toste, F. D.; Michelet, V., Eds. *Gold Catalysis: An Homogeneous Approach*; Imperial College Press: London, U.K., 2014.

(9) Relative solvatochromic values ($E_T^N$) are 0.099 (toluene) and 0.324 (nitrobenzene). For a review, see: Reichardt, C. *Chem. Rev.* **1994**, *94*, 2319.

(10) For examples, see: (a) Margrave, J. L.; Whitmire, K. H.; Hauge, R. H.; Norem, N. T. *Inorg. Chem.* **1990**, *29*, 3252. (b) Zharkova, G. I.; Baldina, I. A.; Igumenov, I. K. *J. Struct. Chem.* **2007**, *48*, 108. (c) Mankad, N. P.; Toste, F. D. *J. Am. Chem. Soc.* **2010**, *132*, 12859.

(11) To discount heterogeneous effects, nanoparticles isolated by heating **1-Br**, **1-Cl** or $Ph_3PAuCF_3$ at 122 °C over 3 days *did not* accelerate the reaction, nor did any solids (unobservable to the naked eye) centrifuged from a reaction halfway to completion. Filtration of reaction mixtures (0.2 $\mu$m PTFE filter) at 50% conversion also did not affect the reaction rates when thermolyses were resumed.

(12) The anodic peak potential of (SIPr)$CuCF_3$ is 0.59 V greater than the potential of (SIPr)$CuCH_3$. Likewise, the anodic peak potential of (dtbpe)$Ni(CF_3)_2$ is 1.17 V greater than the potential of (dtbpe)$Ni(CH_3)_2$. See: Kieltsch, I.; Dubinina, G. G.; Hamacher, C.; Kaiser, A.; Torres-Nieto, J.; Hutchison, J. M.; Klein, A.; Budnikova, Y.; Vicic, D. A. *Organometallics* **2010**, *29*, 1451.

(13) Three-coordinate Au(I) complexes are well-known, and may be coordinatively fluxional in solution. See: Concepción Gimeno, M.; Laguna, A. *Chem. Rev.* **1997**, *97*, 511.

(14) (a) Vicente, J.; Bermudez, M. D.; Escribano, J.; Carrillo, M. P.; Jones, P. G. *J. Chem. Soc., Dalton Trans.* **1990**, 3083. (b) Vicente, J.; Bermudez, M. D.; Escribano, J. *Organometallics* **1991**, *10*, 3380. (c) Wolf, W. J.; Winston, M. S.; Toste, F. D. *Nat. Chem.* **2014**, *6*, 159. (d) Levin, M. D.; Toste, F. D. *Angew. Chem., Int. Ed.* **2014**, *53*, 6211.

(15) $Ph_3PAuF$ and deutero-fluoric (DF) acid are products of $C_{aryl}$−$CF_3$ reductive elimination and tol-$d^8$ activation, respectively. We observe several silylfluoride species by $^{19}$F NMR resulting from facile $Ph_3PAuF$ ionization and quenching of fluoride and DF with the borosilicate NMR tube.

(16) McLinden, M. O.; Splett, J. D. *J. Res. Natl. Inst. Stand. Technol.* **2008**, *113*, 29.

(17) The mechanism of $C_{aryl}$−H activation is unclear. Mechanisms involving electrophilic aromatic substitution have been observed with Au(III), see: (a) Kar, A.; Mangu, N.; Kaiser, H. M.; Tse, M. K. *J. Organomet. Chem.* **2009**, *694*, 524. (b) Ball, L. T.; Lloyd-Jones, G. C.; Russell, C. A. *J. Am. Chem. Soc.* **2014**, *136*, 254. However, although

$PhNO_2$ is substantially less active toward electrophilic aromatic substitution, selectivity for arene activation in $PhNO_2$ increases by a factor of 18 (see Supporting Information). Given the greater acidity of aromatic protons of $PhNO_2$ relative to the deuterons of toluene-$d^8$, we favor a mechanism involving fluoride-assisted deprotonation. We observe no benzylic activation of toluene-$d^8$, suggesting that activation at the arene is kinetically preferred. Such selectivity has been observed in $\sigma$-bond metatheses at late metals, see: (c) Butschke, B.; Schwarz, H. *Organometallics* **2011**, *30*, 1588.

(18) Since [$Ph_3C$−X] = [**2-Cl**], the equilibrium constant expression simplifies to $K_{eq}$ = [**2-X**][$Ph_3C$−Cl]$_o$/[**2-Cl**]$^2$, and can be solved from the relative intensities of $^{19}$F NMR signals for **2-Cl** and **2-Br** or **2-I**.

(19) Domalski, E. S.; Hearing, E. D. *J. Phys. Chem. Ref. Data* **1993**, *22*, 805.

(20) *CRC Handbook of Chemistry and Physics*, 95th ed.; Haynes, W. M., Ed.; CRC Press: Boca Raton, FL, 2015; Section 9, pp 65−68.

(21) The qualitative trend of decreasing Au(III)−X BDEs with higher halides is in marked contrast with gas-phase diatomic Au(I)−X BDEs, which are lowest for Au(I)−Br and highest for Au(I)−Cl and Au(I)−I, see: Reuben Brown, J.; Schwerdtfeger, P.; Schröder, D.; Schwarz, H. *J. Am. Soc. Mass Spectrom.* **2002**, *13*, 485.

(22) Oishi, M.; Yamamoto, H. *Bull. Chem. Soc. Jpn.* **2001**, *74*, 1445.



DOI: 10.1021/jacs.5b04613
*J. Am. Chem. Soc.* 2015, 137, 7921−7928